ENSO Amplitude Modulation Associated with the Mean SST Changes in the Tropical Central Pacific Induced by Atlantic Multidecadal Oscillation

IN-SIK KANG AND HYUN-HO NO

School of Earth and Environmental Sciences, Seoul National University, Seoul, South Korea

FRED KUCHARSKI

Abdus Salam International Centre for Theoretical Physics, Trieste, Italy

(Manuscript received 2 January 2014, in final form 22 July 2014)

ABSTRACT

The mechanism associated with the modulation of the El Niño–Southern Oscillation (ENSO) amplitude caused by the Atlantic multidecadal oscillation (AMO) is investigated by using long-term historical observational data and various types of models. The observational data for the period 1900–2013 show that the ENSO variability weakened during the positive phase of the AMO and strengthened in the negative phase. Such a relationship between the AMO and ENSO amplitude has been reported by a number of previous studies. In the present study the authors demonstrate that the weakening of the ENSO amplitude during the positive phase of the AMO is related to changes of the SST cooling in the eastern and central Pacific accompanied by the easterly wind stress anomalies in the equatorial central Pacific, which were reproduced reasonably well by coupled general circulation model (CGCM) simulations performed with the Atlantic Ocean SST nudged perpetually with the observed SST representing the positive phase of the AMO and the free integration in the other ocean basins. Using a hybrid coupled model, it was determined that the mechanism associated with the weakening of the ENSO amplitude is related to the westward shift and weakening of the ENSO zonal wind stress anomalies accompanied by the westward shift of precipitation anomalies associated with the relatively cold background mean SST over the central Pacific.

1. Introduction

The North Atlantic Ocean sea surface temperature (SST) exhibits a multidecadal variability called the Atlantic multidecadal oscillation (AMO), which has been described by observational and modeling studies (Kerr 2000; Delworth and Mann 2000; Knight et al. 2005). Many studies have suggested that the multidecadal SST variability over the North Atlantic is linked to multidecadal fluctuations of the Atlantic meridional overturning circulation (AMOC) (Delworth and Mann 2000; Knight et al. 2005; Zhang and Delworth 2007; Wang et al. 2010, Polo et al. 2013). Recent decades after 1995, a positive phase of the AMO accompanied by SST warming over the northern Atlantic has occurred. In the same period, the El Niño–Southern Oscillation (ENSO) variability has been weakened (Xiang et al. 2013; Chung and Li 2013). Although the impact of the AMO in the ENSO amplitude has been demonstrated by a number of previous studies (Dong et al. 2006; Timmermann et al. 2007; Dong and Sutton 2007; and others), the mechanism behind the relationship between the AMO and ENSO amplitude is not yet understood at present.

The linkage between the variability of the Atlantic SST and ENSO through an atmospheric bridge has been suggested by observational studies and coupled GCM (CGCM) experiments (Dong et al. 2006; Timmermann et al. 2007; Dong and Sutton 2007; Rodríguez-Fonseca et al. 2009; López-Parages and Rodríguez-Fonseca 2012; Kayano and Capistrano 2014; Keenlyside et al. 2013; Svendsen et al. 2013). Using observed data, Rodríguez-Fonseca et al. (2009) and Jansen et al. (2009) demonstrated the relationship between the tropical Atlantic and Pacific Oceans, with Atlantic SST anomalies leading Pacific SST anomalies by 6 months. Rodríguez-Fonseca et al. (2009) and Ding et al. (2012) showed that SST warming over the equatorial Atlantic strengthens the

Corresponding author address: In-Sik Kang, School of Earth and Environmental Sciences, Seoul National University, San 56-1, Sillim-dong, Gwanak-gu, Seoul 151-747, South Korea.
E-mail: kang@climate.snu.ac.kr

DOI: 10.1175/JCLI-D-14-00018.1

Walker circulation over the tropical Pacific, which subsequently produces strong easterly wind anomalies over the central Pacific after several months. Dong et al. (2006) and others showed that the positive phase of the AMO accompanies relatively weak ENSO variability by using coupled GCM simulations with the Atlantic Ocean SSTs relaxed to those of the positive phase of the AMO. Subsequently, Dong and Sutton (2007) and others showed with coupled model experiments that increases of freshwater flux in the North Atlantic Ocean results in the weakening of AMOC, which influences the Pacific mean states and in turn induces enhancement of ENSO variability. Those studies mentioned above indicate that the tropical Atlantic SST changes with both multidecadal and interannual time scales influence the climate states in the tropical Pacific and that the modulation of ENSO amplitude with multidecadal time scales is through the changes of the mean state in the tropical Pacific induced by the tropical Atlantic SST changes.

The Pacific climatological mean climate, particularly SSTs, has been known to influence the ENSO amplitude (An and Wang 2000; Yeh and Kirtman 2005; Kim et al. 2011; Xiang et al. 2013; Chung and Li 2013). Recently, Chung and Li demonstrated that the modulation of the ENSO amplitude is associated with decadal changes in the mean SST over the tropical Pacific, particularly through changes in the east–west gradient of the tropical Pacific SSTs and the precipitation changes associated with it. By using coupled model experiments with different parameter values for the convection scheme, Kim et al. (2011) showed that the ENSO amplitude is sensitive to the mean precipitation over the eastern Pacific: increased mean precipitation over the eastern Pacific results in an increase in the ENSO amplitude. In their study, the increased mean precipitation over the eastern Pacific induced an eastward shift of the ENSO atmospheric component, particularly the zonal wind stress anomaly, that then resulted in stronger ENSO variability. Although those studies suggested that the changes in the mean SST and precipitation in the tropical Pacific can modify the ENSO amplitude through a zonal shift of ENSO atmospheric components, the mechanism underlying this phenomenon was not clearly demonstrated in the previous studies. The study by Kang and Kug (2002) may provide a clue to the mechanism. They showed that the ENSO amplitude is very sensitive to the location of the zonal wind stress anomalies associated with ENSO since the negative feedback by the delayed oscillator mechanism depends on the oceanic Rossby wave excited by the wind stress anomalies in the equatorial central Pacific (Suarez and Schopf 1988). When the zonal wind stress anomalies associated with ENSO are shifted to the west, the negative feedback by Rossby waves is stronger than that of the Rossby waves excited by the zonal wind stress anomalies in the central Pacific; therefore, the ENSO amplitude is limited and thus relatively weak.

In the present study, we provide additional evidence for the association of ENSO amplitude modulation with the AMO using long-term observational data and a coupled GCM. In addition, we demonstrate that the positive phase of the AMO accompanies SST cooling in the tropical central Pacific, which results in the westward shift of zonal wind stress anomalies associated with the ENSO SST anomaly. We further demonstrate here that the zonal displacement of the ENSO wind stress anomalies serves as a mechanism for the ENSO amplitude modulation associated with the AMO. Section 2 describes the data and models used. The changes in mean climate in the Pacific and the ENSO variability associated with changes in the AMO are presented in section 3. The mechanism related to the ENSO amplitude modulation is investigated in section 4, and a summary and a discussion are presented in section 5.

2. Data and models

The monthly-mean SST data from January 1900 to May 2013 used in the present study were obtained from the National Oceanic and Atmospheric Administration extended reconstructed SST, version 3 (ERSST.v3) (Smith et al. 2008). The horizontal resolution of the SST data is 2° latitude × 2° longitude. The precipitation data from January 1979 to May 2013 were obtained from the Global Precipitation Climatology Project (GPCP) (Adler et al. 2003). The horizontal resolution of the GPCP precipitation data is 2.5° latitude × 2.5° longitude. We also used the monthly-mean 850-hPa zonal wind data from January 1948 to May 2013 obtained from the National Centers for Environmental Prediction–National Center for Atmospheric Research (NCEP–NCAR) reanalysis (Kalnay et al. 1996). The horizontal resolution of 850-hPa zonal wind data is 2.5° latitude × 2.5° longitude. Linear trends of all observational data were removed, and the average of the monthly-mean data from June to May of the next year was used as an annual mean.

The coupled general circulation model used in this study is the Seoul National University (SNU) CGCM (Kug et al. 2008; Kim et al. 2008; Ham et al. 2012). The atmospheric portion of the model (AGCM) has a spectral resolution of T42 and 20 vertical sigma levels. The physics of the model includes parameterizations of convections, radiation, planetary boundary layers (PBL), and land surfaces. The deep convection scheme

is a simplified Arakawa–Schubert scheme (Numaguti et al. 1995), the boundary layer scheme is a nonlocal diffusion scheme described by Holtslag and Boville (1993), and the radiation processes are parameterized by the two-stream k-distribution scheme implemented by Nakajima et al. (1995). The land surface processes are represented by the land surface model of Bonan (1996), which was developed at the National Center for Atmospheric Research. A detailed description of physical parameterizations in the AGCM can be found in Lee et al. (2001, 2003). The oceanic portion of the model is the Modular Ocean Model, version 2.2 (MOM 2.2) developed at the Geophysical Fluid Dynamics Laboratory of Princeton University. The zonal resolution is 1° and the meridional resolution is ⅓° between 8°S and 8°N, gradually increasing to 3° in the extratropics. The vertical levels are configured with 23 levels in the upper 450 m and with a 10-m thickness of the top 10 layers. The mixed layer ocean model (Noh and Kim 1999) is embedded in the present ocean model. The air–sea coupling interval of the coupled model is 2 h (Ham et al. 2012). No flux correction is applied, and the model does not show significant climate drift in free long-term integrations.

Another model used in this study is a hybrid coupled model (Kang and Kug 2000). The oceanic component of the model is based on an intermediate ocean model similar to the Cane–Zebiak (CZ) ocean model (Cane and Zebiak 1987). The present model differs from the CZ model by a modification of the subsurface temperature formula. The formula used in the present model is based on a statistical relationship between the subsurface temperature and thermocline depth, which were obtained from the NCEP ocean assimilation data. The atmospheric component of the hybrid coupled model provides the wind stress anomalies to force the ocean model, which was computed as a function of model Niño-3 SST anomalies. Details of the model can be obtained in Kang and Kug (2000, 2002).

3. Changes of mean climate in the Pacific and the ENSO variability associated with the AMO

The changes in the Pacific mean climate and the ENSO amplitude associated with the Atlantic SST anomalies related to the Atlantic multidecadal oscillation were analyzed with long-term observational data, and the changes were then reproduced with the CGCM. The AMO is known to be linked to the strengthening and weakening of the Atlantic meridional overturning circulation (Delworth and Mann 2000; Knight et al. 2005; Zhang and Delworth 2007; Wang et al. 2010). A strengthened AMOC leads to large meridional heat transport from the equator to high latitudes and causes

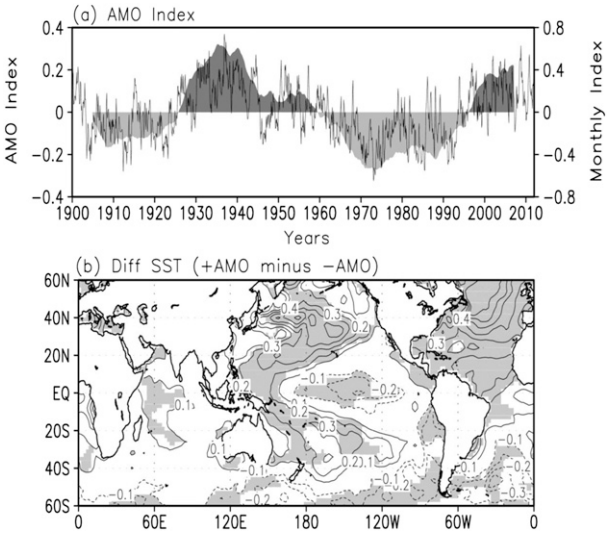

FIG. 1. (a) Time series of the AMO index smoothed with a 121-month running mean (°C, shading) and its monthly index (°C, black solid line). The AMO index is obtained by averaging SST anomalies over the NH Atlantic Ocean. (b) Difference map between the mean SSTs during positive phases of the AMO and those of the negative phases of the AMO. Shading indicates differences above the 95% statistically significant level.

SST warming over the whole northern Atlantic. In the present study, we defined the AMO index as the 121-month running mean of the detrended SST anomalies averaged over the North Atlantic region (0°–60°N, 70°W–0°) (Knight et al. 2005; Sutton and Hodson 2005). The AMO index, obtained by applying a 121-month running mean, is shown in Fig. 1a with shading. The monthly index without the smoothing is also presented in the figure with a solid line. The monthly index shows large interannual variation, whereas the AMO index clearly shows the multidecadal variations with a positive phase in a recent decade (Enfield et al. 2001; Knight et al. 2005; Sutton and Hodson 2005). Consecutive 15-yr periods were chosen to define the positive and negative phases of the AMO, with the periods 1930–45 and 1998–2013 defining the positive phases and those of 1904–19 and 1979–94 defining the negative phases. Figure 1b shows the global distribution of the SST differences between the average values for the two positive phases and negative phases. The SST difference map shows that the positive phase of the AMO has accompanied relatively large SST anomalies of more than 0.5°C in the extratropical Pacific and high-latitude Northern Atlantic Ocean, and positive SST anomalies in the tropical Atlantic Ocean and negative SST anomalies in the central tropical Pacific. The spatial pattern of the map is similar to that of the SST anomalies averaged for recent decades, as seen in Fig. 2. Because precipitation data are available after 1979, the difference maps of SST

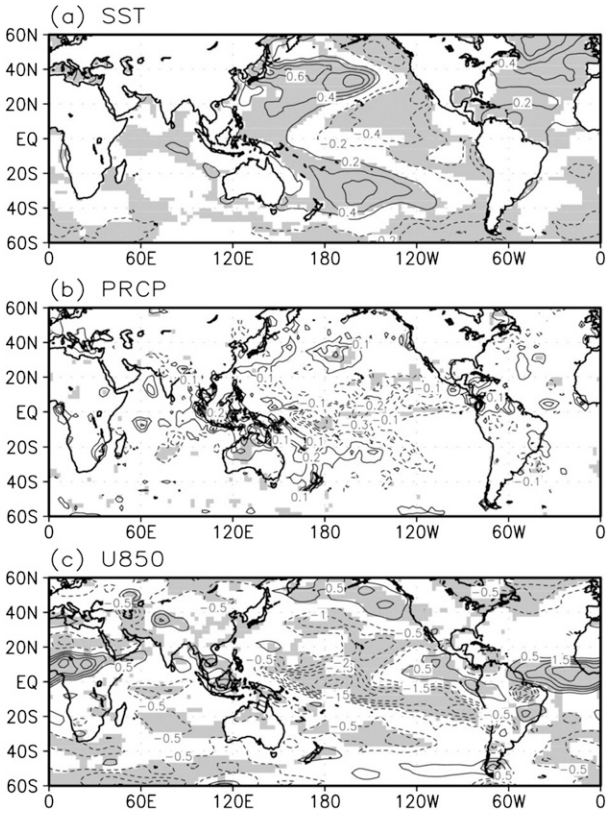

FIG. 2. Difference maps between the mean states for June 1998–May 2013 and for June 1979–May 1994: (a) SST (°C), (b) precipitation (mm day^{-1}), and (c) 850-hPa zonal wind (m s^{-1}). Shading indicates differences above the 95% significant level.

(Fig. 2a), precipitation (Fig. 2b), and 850-hPa zonal wind (Fig. 2c) between the two recent periods of 1998–2013 (the positive phase) and 1979–94 (the negative phase) were obtained and are shown in Fig. 2. In the recent decade, relatively large warming was appeared in the Northern Atlantic Ocean and the western extratropical Pacific in the Northern and Southern Hemispheres. On the other hand, significant SST cooling (from about −0.3° to −0.5°C) also appeared in the central Pacific. As will be discussed in the next section, this central Pacific SST change is a crucial factor for modulating the ENSO variability. Associated with the SST changes, notable changes in precipitation and lower-level wind anomalies occurred in the tropical Pacific, as shown by Hong et al. (2013). The most notable changes are easterly wind anomalies stronger than 2 m s^{-1} in the central equatorial Pacific and the dry and wet anomalies in the tropical central and western Pacific, respectively. The mechanism underlying the changes in SST, wind, and precipitation in the Pacific associated with the recent AMO is well described in Hong et al. (2013).

The ENSO variability for different AMO phases is analyzed and plotted in Fig. 3. Figures 3a and 3c show the standard deviations of SST anomalies in the negative phases of the AMO for 1904–19 and 1979–94, respectively, and Figs. 3b and 3d show the standard deviations of SST anomalies in the positive phases of the AMO for 1930–45 and 1998–2013. The SST variability in the positive phases of the AMO is clearly weaker than the variability in the negative phases (Fig. 3e). In addition, the center of the SST anomaly moved to the central Pacific during the El Niño events in the recent decade, as shown by Xiang et al. (2013) and Chung and Li (2013).

We performed two CGCM experiments to investigate the extent to which the observed changes over the Pacific (as mentioned above) were associated with the AMO. In the first experiment, the Atlantic SST was nudged with the seasonally varying climatological SST obtained from a 100-yr free run, whereas the other oceans were run freely [the control (CNT) run]. The second experiment is the same as the CNT run except that the Atlantic SST was nudged with the model climatological cycle and the SST anomalies (the AMO run), whose spatial pattern is the same as that of the positive phase of the AMO shown in Fig. 1b, but that their magnitudes were multiplied by a factor of 2 to produce a clear signal associated with the Atlantic SST anomalies. Therefore, the difference between the AMO and CNT runs indicates the global climate anomalies induced purely by the Atlantic SST anomalies associated with the AMO. The nudging time scale used here is 1 day so that the simulated SST state in the Atlantic was kept, more or less, in a state of the nudged SST. Both runs were integrated for 180 years and the model data produced for last 150 years were used in the present study.

Figure 4 shows the mean state differences averaged for 150 years between the AMO and CNT runs. As expected, the SST differences in the Atlantic Ocean are almost the same as the nudged SST anomalies, except that the simulated differences are 2 times larger than the observed differences. A relatively large SST warming is generated in the extratropical western Pacific in the Northern Hemisphere (NH). The magnitude of the SST warming is about the same as that in Fig. 2. Considering that the nudged SST in the Atlantic Ocean is 2 times bigger than that of Fig. 2, the result mentioned above indicates that about a half of the NH SST anomalies in Fig. 2 can be related to the Atlantic SST anomalies. On the other hand, a significant SST cooling (cooler than −0.5°C) is also generated in the central tropical Pacific. Half of the cooling is about 70% of the negative SST anomalies recently appeared in the central tropical Pacific, shown in Fig. 2, indicating that a large part of the recent cooling could be related to the Atlantic warming associated with the positive phase of the AMO.

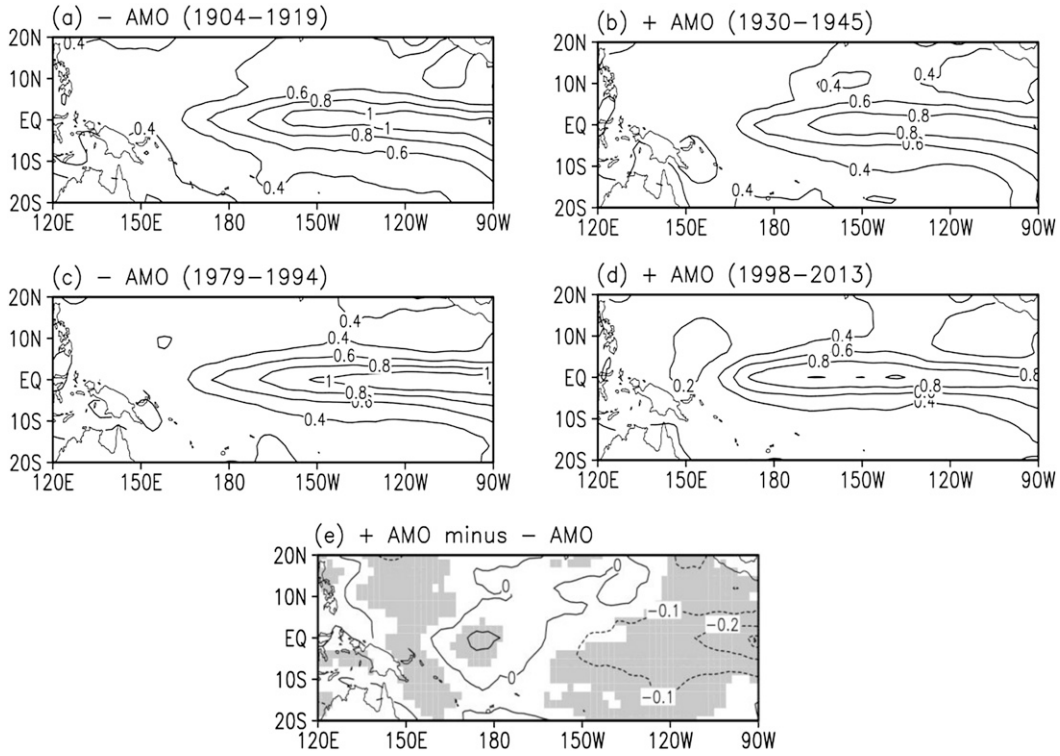

FIG. 3. Spatial patterns of the standard deviations of detrended SST anomalies over the tropical Pacific during the negative phase of the AMO of (a) 1904–19 and (c) 1979–94. (b),(d) Positive phase of the AMO of 1930–45 and 1998–2013. (e) Difference between the positive and the negative phase of the AMO. Shading indicates significant differences at the 95% confidence level using an *F* test.

Figures 4b and 4c show the simulated differences of precipitation and the 850-hPa zonal wind. The dry (wet) anomalies are generated in the tropical central (western) Pacific, whose spatial pattern is similar to that of Fig. 2b. The easterly wind anomalies of about 4 m s^{-1} are generated in the central and western Pacific, whose spatial pattern and magnitude (half is 2 m s^{-1}) are similar to that of the easterly wind anomalies in the tropical Pacific shown in Fig. 2c. It is noted that the equatorial easterly anomalies induce upwelling by the Ekman drift; thus, the cooling is generated in the central tropical Pacific as seen in Fig. 4a. Overall, the CGCM results mentioned above indicate that a large fraction of the observed mean changes in the tropical Pacific for recent decades is related to the AMO.

The ENSO variability for the CNT run and the AMO run, analyzed in terms of standard deviations of the SST anomalies over the tropical Pacific, is shown in Figs. 5a and 5b. The ENSO variability is clearly lower in the AMO run (the maximum value of 1.3°C) than in the CNT run (the maximum value of 1.7°C). This result is consistent with those of previous studies based on observational data and other CGCMs (Dong et al. 2006; Timmermann et al. 2007; Kayano and Capistrano 2014). The zonal wind stress anomalies associated with ENSO were obtained by regressing the simulated Niño-3 index, which is the SST anomaly averaged over the region of 5°S–5°N, 150°–90°W on the zonal wind stress anomalies simulated over the tropical Pacific. The results for the CNT and AMO runs are shown in Figs. 6a and 6b. The most distinctive difference between the ENSO zonal wind stress anomalies of the AMO and CNT runs appears in the zonal location of the zonal wind stress anomalies. The location of the anomaly center in the AMO run (165°E) is shifted to the west compared to that of the CNT run (180°). The relatively small ENSO amplitude accompanied by the westward shift of zonal wind stress anomalies can be understood in terms of stronger negative feedback of the delayed oscillator mechanism described by Kang and Kug (2002) (see section 1). It is also noted that the ENSO zonal wind stress anomalies in the AMO run are less effective at increasing the thermocline anomalies in the eastern Pacific compared to those in the CNT run, as seen in Fig. 7. The westward shift of ENSO zonal wind stress anomalies in the AMO run results in smaller thermocline depth anomalies in the eastern Pacific, which lead to smaller SST variability in the eastern Pacific. Thus, the westward shift of the

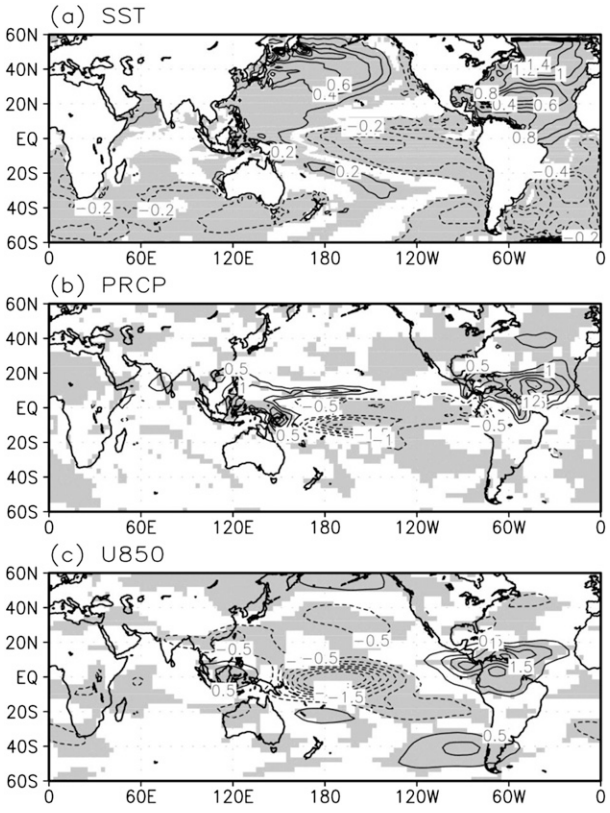

FIG. 4. Difference maps of (a) SST (°C), (b) precipitation (mm day^{-1}), and (c) 850-hPa zonal wind (m s^{-1}) between the CGCM experiments of the CNT and AMO runs. Shading indicates differences above the 95% significant level.

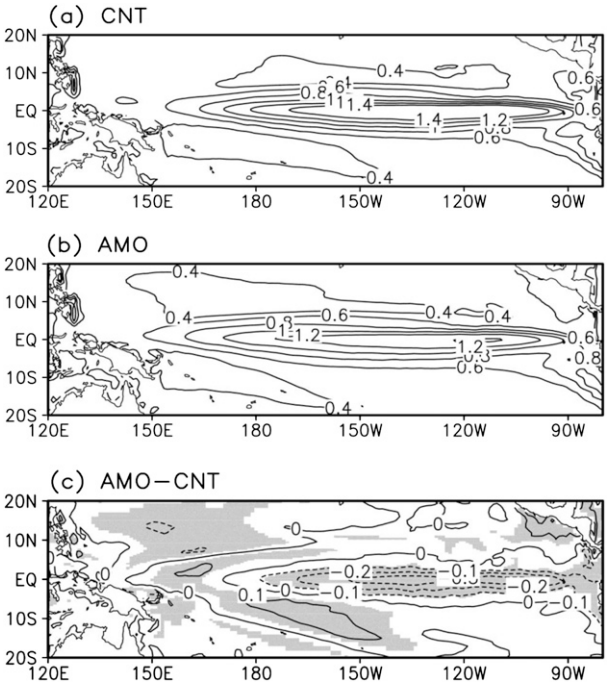

FIG. 5. Spatial patterns of the standard deviations of monthly SST anomalies (°C) over the tropical Pacific of (a) CNT and (b) AMO: (c) difference between the CNT and AMO runs. Shading indicates significant differences at the 95% confidence level using an F test.

ENSO zonal wind stress anomalies appears to be a crucial factor in reducing the ENSO amplitude during the positive phase of the AMO. However, questions remain as to why the westward shift of the ENSO wind stress anomalies occurs in the positive phase of the AMO and why it reduces the ENSO amplitude. In the next section, we address these questions by using various model experiments.

4. A mechanism for ENSO weakening in the positive phase of the AMO

In this study, we propose that the SST cooling in the central Pacific is responsible for the westward shift of the ENSO zonal wind stress anomalies during the positive phase of the AMO. To confirm this hypothesis, we performed two sets of AGCM experiments to investigate how different zonal wind stress anomalies respond to the same SST anomaly with different background mean SST states over the tropical Pacific. Two AGCM experiments in the first set are carried out with two different SSTs: one with the observed climatological SST (CNT1) and the other with the same climatological SST plus the El Niño SST anomaly (ENT1) as shown in Fig. 8a. The El Niño SST anomaly during the averaged state of El Niño for 1900–2013 is obtained from the first EOF of tropical Pacific SST anomalies. All experiments were integrated

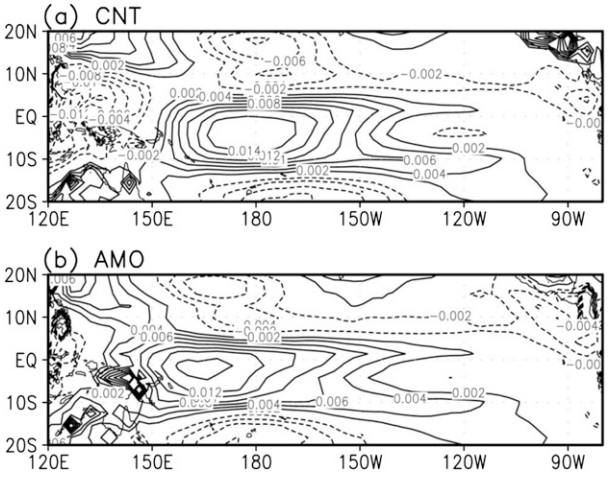

FIG. 6. Regression maps of the zonal wind stress anomalies (N m^{-2} °C^{-1}) in the tropical Pacific against the normalized Niño-3 index, obtained from the CGCM simulations for (a) CNT and (b) AMO.

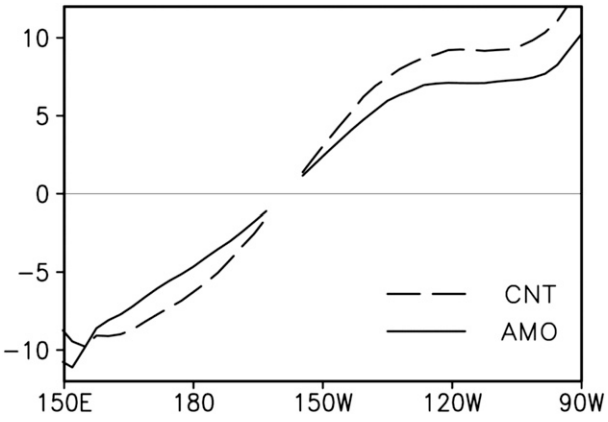

FIG. 7. Zonal structure of the thermocline depth anomalies (m) during the El Niño along the equator (5°S–5°N) obtained by regressing the simulated Niño-3 index on the thermocline depth anomalies of the CNT (dashed line) and AMO (solid line) runs. Significant values above the 95% significant level are indicated.

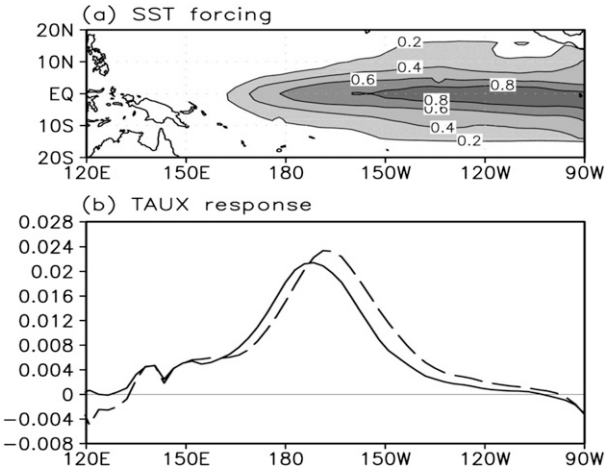

FIG. 8. (a) SST anomalies during the average state of El Niño for 1900–2013, obtained from the first EOF of tropical Pacific SST anomalies. (b) Zonal wind stress anomalies ($N\,m^{-2}$) along the equator (5°S–5°N), simulated by an AGCM with two different SSTs prescribed. Two AGCM experiments were performed with the same SST anomalies shown in (a) in addition to the two different climatological SSTs. Dashed and solid lines indicate the observed climatological SST and the same climatological SST plus the relatively cold SST anomalies over the central Pacific obtained by the SST difference between the CGCM experiments of the CNT and AMO runs, respectively. Refer to the text.

for 50 years and the last 30 years of data were used in the analysis. The zonal wind stress anomalies forced by the El Niño SST anomaly under the observed climatological mean SST condition obtained by ENT1 − CNT1 is indicated by the dashed line in Fig. 8b. The second set of AGCM experiments (CNT2 and ENT2) is the same as the first set except that the cold SST anomalies in the central Pacific simulated by the AMO run, which are shown in the previous section, are included in the climatological mean SST. Thus, the difference between ENT2 and CNT2 provides the atmospheric anomalies forced by the same El Niño SST anomaly as that of ENT1 but under the climatological tropical Pacific conditions influenced by the AMO. The zonal wind stress anomalies obtained by ENT2 − CNT2 are shown by the solid line in Fig. 8b. The ENSO-related zonal wind stress anomalies under the climatological mean SST state during the positive phases of the AMO (175°W) are indeed shifted slightly to the west compared to and are weaker than those of the ENSO wind stress anomalies under the climatological mean state without the cooling in the central Pacific (165°W), confirming that the slight cooling in the tropical central Pacific is responsible for the westward shift of the ENSO-related zonal wind stress anomalies in the tropical Pacific. This result can be interpreted as follows: in the case of SST cooling located in the central pacific (the AMO state), the positive SST anomalies are less effective at increasing anomalous convection in the central Pacific (Kim et al. 2011; Chung and Li 2013). Thus, the ENSO-related precipitation anomalies for the AMO state are shifted to the west toward the warm pool region compared to the ENSO anomalies in the normal climatological mean state, and the zonal wind stress anomalies associated with the precipitation anomalies are also shifted to the west. It should be noted that the westward shift of the zonal wind stress anomalies is not as strong as in the simulation in the coupled model shown in the previous section; this difference might be caused by a lack of ocean–atmosphere feedback in the present AGCM experiments. It is also worth mentioning, with the same reason (SST cooling in the central Pacific) mentioned above, that the ENSO wind stress anomalies for the positive phase of the AMO are weaker than those of the normal state, as seen in Fig. 8b. These weaker wind stress anomalies also influence the weaker ENSO amplitude in the positive phase of the AMO.

In particular, the zonal shift of the ENSO zonal wind stress anomalies can influence the ENSO amplitude, which was demonstrated by Kang and Kug (2002). Here, we assessed the impact of the westward shift of the ENSO zonal wind stress anomalies on the ENSO amplitude using a hybrid coupled model similar to that of Kang and Kug, which was described in section 2. The only difference between their model and the present model is the function of the wind stress anomaly, which is computed by using the following formula:

$$\tau(x,y,t) = \alpha F(x,y)T(t), \qquad (1)$$

where $T(t)$ is the model-produced Niño-3 SST anomaly in which the zonal wind stress anomalies are proportional

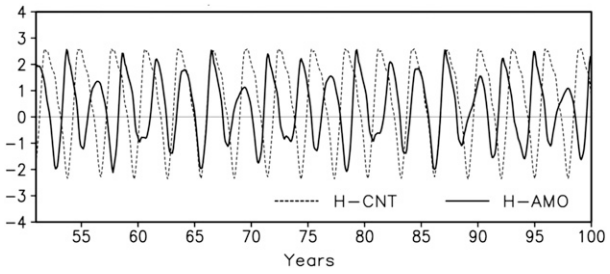

FIG. 9. Time series of Niño-3 SST anomalies simulated a hybrid coupled model with two different wind stress functions. Dotted and solid lines denote the zonal wind stress functions whose spatial patterns are same as those of Figs. 6a and 6b, respectively.

to the Niño-3 SST anomaly, α is the scaling coefficient (which is 0.4 as used by Kang and Kug 2002), and $F(x, y)$ is the spatial function of the zonal wind stress anomalies. The spatial distributions of the wind stress functions are the same as those of Figs. 6a and 6b, which are the ENSO-related zonal wind stress anomalies of the control and the AMO coupled model experiments, respectively, described in the previous section. Two hybrid coupled model experiments, referred to as the H-CNT and H-AMO runs, were carried out with the two different zonal wind stress functions of Figs. 6a and 6b. Both runs were integrated for 100 years, and the model data produced for last 50 years were used for the following analysis. The time series of the Niño-3 SST anomaly produced by the hybrid coupled model are shown in Fig. 9. The dotted (solid) lines indicate the H-CNT (H-AMO) runs. The ENSO amplitude in the H-AMO run is clearly weaker than that of the H-CNT run. The standard deviation of the monthly Niño-3 SST index produced by the H-AMO run (1.34°C) is decreased by 19% compared to that of the H-CNT run (1.65°C), confirming that the westward shift of the ENSO zonal wind stress anomalies plays a key role in the weakening of the ENSO amplitude.

5. Summary and discussion

The mechanism for modulating the ENSO amplitude associated with the Atlantic multidecadal oscillation was investigated using long-term observational data and CGCM experiments. Since the mid-1990s, the Atlantic Ocean has experienced warming in the Northern Hemisphere and the SST cooling has been observed together with the easterly wind anomalies in the tropical central Pacific. These observed anomalies in the Pacific are reproduced reasonably well by the present CGCM experiment in which the Atlantic SSTs are nudged with those representing the positive phase of the AMO. The observation data and coupled model experiments also show that the ENSO variability associated with the positive phase of the AMO is weaker than those of other periods. These results are consistent with previous observational and model studies (Timmermann et al. 2007; Dong and Sutton 2007; Kayano and Capistrano 2014). Here, we further investigated the mechanism related to the weakening of the ENSO amplitude during the positive phase of the AMO.

The westward shift of the ENSO zonal wind anomalies in the tropical Pacific is a crucial factor for weakening of the ENSO variability during the positive phase of the AMO. The westward shift of the ENSO zonal wind stress anomalies resulted from a slight cooling of the mean SSTs in the tropical central Pacific during the positive phase of the AMO. The effect of the mean SST cooling could be interpreted as follows: with the relatively cold mean SST in the central pacific, the positive ENSO SST anomalies are less effective at producing anomalous convection in the central Pacific (Kim et al. 2011; Chung and Li 2013). Thus, the ENSO-related precipitation anomalies should be shifted to the west toward the warm pool region compared to those of other periods, and the zonal wind stress anomalies associated with the precipitation anomalies are also shifted to the west. The ENSO amplitude modulation by the zonal displacement of ENSO-related zonal wind stress anomalies is further demonstrated by using a hybrid coupled model in the present study.

From the delayed oscillator mechanism (Suarez and Schopf 1988; Cane et al. 1990), the negative feedback and the decay of ENSO depend on the off-equatorial Rossby waves excited by the ENSO-related equatorial wind stress anomalies. When the center of the zonal wind stress anomalies is shifted to the west, the distance for the Rossby waves to reach the western boundary is shortened (Kang and An 1998; An and Wang 2000; and others), so the Rossby waves at the western boundary (WB) are less damped because of a shorter travel distance; then the Kelvin wave reflected by the Rossby waves at the WB can more effectively damp the preexisting Kelvin waves in the eastern Pacific. This stronger negative feedback results in weakening of the ENSO amplitude during the positive phase of the AMO.

The westward shift of the ENSO atmospheric anomalies could explain the frequent occurrence of the so-called central Pacific El Niño events in recent decades (Xiang et al. 2013; Chung and Li 2013). The mean SST cooling in the central Pacific could be an important cause for the westward shift of the ENSO atmospheric anomalies. Xiang et al. has suggested that the central Pacific El Niño events will increase in the coming decades if the relatively cold mean SSTs persist over the central-eastern Pacific. The present study demonstrates

that the SST cooling in the central Pacific that occurred in recent decades is associated with the warming of northern Atlantic SST associated with a positive phase of the AMO and thus suggests that the frequent occurrence of the central Pacific El Niño in a recent decade may be related to the positive phase of the AMO in the Atlantic Ocean. However, a further study may be needed to clearly understand the relationship between the central Pacific El Niño and the AMO.

Acknowledgments. This work was supported by a National Research Foundation of Korea Grant funded by the Korean Government (MEST) (NRF-2012M1A2A2671775) and by the Brain Korea 21 Program for Leading Universities and Students (PLUS) Project.

REFERENCES

Adler, R. F., and Coauthors, 2003: The Version-2 Global Precipitation Climatology Project (GPCP) monthly precipitation analysis (1979–present). *J. Hydrometeor.,* **4,** 1147–1167, doi:10.1175/1525-7541(2003)004<1147:TVGPCP>2.0.CO;2.

An, S.-I., and B. Wang, 2000: Interdecadal change of the structure of the ENSO mode and its impact on the ENSO frequency. *J. Climate,* **13,** 2044–2055, doi:10.1175/1520-0442(2000)013<2044:ICOTSO>2.0.CO;2.

Bonan, G. B., 1996: A land surface model (LSM version 1.0) for ecological, hydrological, and atmospheric studies: Technical description and user's guide. NCAR Tech. Note NCAR/TN-417+STR, 50 pp. [Available online at http://nldr.library.ucar.edu/repository/assets/technotes/TECH-NOTE-000-000-000-229.pdf.]

Cane, M. A., and S. E. Zebiak, 1987: Prediction of El Niño events using a physical model. *Atmosphere and Ocean Variability,* H. Cattel, Ed., Royal Meteorological Society Press, 153–182.

——, M. Münnich, and S. E. Zebiak, 1990: A study of self-excited oscillations of the tropical ocean–atmosphere system. Part I: Linear analysis. *J. Atmos. Sci.,* **47,** 1562–1577, doi:10.1175/1520-0469(1990)047<1562:ASOSEO>2.0.CO;2.

Chung, P.-H., and T. Li, 2013: Interdecadal relationship between the mean state and El Niño types. *J. Climate,* **26,** 361–379, doi:10.1175/JCLI-D-12-00106.1; Corrigendum, **26,** 2700, doi:10.1175/JCLI-D-13-00112.1.

Delworth, T. L., and M. E. Mann, 2000: Observed and simulated multidecadal variability in the Northern Hemisphere. *Climate Dyn.,* **16,** 661–676, doi:10.1007/s003820000075.

Ding, H., N. S. Keenlyside, and M. Latif, 2012: Impact of the equatorial Atlantic on the El Niño Southern Oscillation. *Climate Dyn.,* **38,** 1965–1972, doi:10.1007/s00382-011-1097-y.

Dong, B., and R. T. Sutton, 2007: Enhancement of ENSO variability by a weakened Atlantic thermohaline circulation in a coupled GCM. *J. Climate,* **20,** 4920–4939, doi:10.1175/JCLI4284.1.

——, ——, and A. A. Scaife, 2006: Multidecadal modulation of El Niño–Southern Oscillation (ENSO) variance by Atlantic Ocean sea surface temperatures. *Geophys. Res. Lett.,* **33,** L08705, doi:10.1029/2006GL025766.

Enfield, D. B., A. M. Mestas-Nuñez, and P. J. Trimble, 2001: The Atlantic multidecadal oscillation and its relation to rainfall and river flows in the continental U.S. *Geophys. Res. Lett.,* **28,** 2077–2080, doi:10.1029/2000GL012745.

Ham, Y.-G., I.-S. Kang, D. Kim, and J.-S. Kug, 2012: El-Nino Southern Oscillation simulated and predicted in SNU coupled GCMs. *Climate Dyn.,* **38,** 2227–2242, doi:10.1007/s00382-011-1171-5.

Holtslag, A. A. M., and B. A. Boville, 1993: Local versus nonlocal boundary-layer diffusion in a global climate model. *J. Climate,* **6,** 1825–1842, doi:10.1175/1520-0442(1993)006<1825:LVNBLD>2.0.CO;2.

Hong, S., I.-S. Kang, I. Choi, and Y.-G. Ham, 2013: Climate responses in the tropical Pacific associated with Atlantic warming in recent decades. *Asia-Pac. J. Atmos. Sci.,* **49,** 209–217, doi:10.1007/s13143-013-0022-1.

Jansen, M. F., D. Dommenget, and N. Keenlyside, 2009: Tropical atmosphere–ocean interactions in a conceptual framework. *J. Climate,* **22,** 550–567, doi:10.1175/2008JCLI2243.1.

Kalnay, E., and Coauthors, 1996: The NCEP/NCAR 40-Year Reanalysis Project. *Bull. Amer. Meteor. Soc.,* **77,** 437–471, doi:10.1175/1520-0477(1996)077<0437:TNYRP>2.0.CO;2.

Kang, I.-S., and S.-I. An, 1998: Kelvin and Rossby wave contributions to the SST oscillation of ENSO. *J. Climate,* **11,** 2461–2469, doi:10.1175/1520-0442(1998)011<2461:KARWCT>2.0.CO;2.

——, and J.-S. Kug, 2000: An El-Nino prediction system using an intermediate ocean and a statistical atmosphere. *Geophys. Res. Lett.,* **27,** 1167–1170, doi:10.1029/1999GL011023.

——, and ——, 2002: El Niño and La Niña sea surface temperature anomalies: Asymmetry characteristics associated with their wind stress anomalies. *J. Geophys. Res.,* **107,** 4372, doi:10.1029/2001JD000393.

Kayano, M. T., and V. B. Capistrano, 2014: How the Atlantic multidecadal oscillation (AMO) modifies the ENSO influence on the South American rainfall. *Int. J. Climatol.,* **34,** 162–178, doi:10.1002/joc.3674.

Keenlyside, N. S., H. Ding, and M. Latif, 2013: Potential of equatorial Atlantic variability to enhance El Niño prediction. *Geophys. Res. Lett.,* **40,** 2278–2283, doi:10.1002/grl.50362.

Kerr, R. A., 2000: A North Atlantic climate pacemaker for the centuries. *Science,* **288,** 1984–1986, doi:10.1126/science.288.5473.1984.

Kim, D., J.-S. Kug, I.-S. Kang, F.-F. Jin, and A. T. Wittenberg, 2008: Tropical Pacific impacts of convective momentum transport in the SNU coupled GCM. *Climate Dyn.,* **31,** 213–226, doi:10.1007/s00382-007-0348-4.

——, Y.-S. Jang, D.-H. Kim, Y.-H. Kim, M. Watanabe, F.-F. Jin, and J.-S. Kug, 2011: El Niño–Southern Oscillation sensitivity to cumulus entrainment in a coupled general circulation model. *J. Geophys. Res.,* **116,** D22112, doi:10.1029/2011JD016526.

Knight, J. R., R. J. Allan, C. K. Folland, M. Vellinga, and M. E. Mann, 2005: A signature of persistent natural thermohaline circulation cycles in observed climate. *Geophys. Res. Lett.,* **32,** L20708, doi:10.1029/2005GL024233.

Kug, J.-S., J.-Y. Lee, I.-S. Kang, B. Wang, and C.-K. Park, 2008: Optimal multi-model ensemble method in seasonal climate prediction. *Asia-Pac. J. Atmos. Sci.,* **44,** 259–267.

Lee, M.-I., I.-S. Kang, J.-K. Kim, and B. E. Mapes, 2001: Influence of cloud-radiation interaction on simulating tropical intraseasonal oscillation with an atmospheric general circulation model. *J. Geophys. Res.,* **106,** 14 219–14 233, doi:10.1029/2001JD900143.

——, ——, and B. E. Mapes, 2003: Impacts of cumulus convection parameterization on aqua-planet AGCM Simulations of

tropical intraseasonal variability. *J. Meteor. Soc. Japan,* **81,** 963–992, doi:10.2151/jmsj.81.963.

López-Parages, J., and B. Rodríguez-Fonseca, 2012: Multidecadal modulation of El Niño influence on the Euro-Mediterranean rainfall. *Geophys. Res. Lett.,* **39,** L02704, doi:10.1029/2011GL050049.

Nakajima, T., M. Tsukamoto, Y. Tsushima, and A. Numaguti, 1995: Modelling of the radiative processes in an AGCM. *Climate System Dynamics and Modelling,* T. Matsuno, Ed., Vol. 3, University of Tokyo, 104–123.

Noh, Y., and H. J. Kim, 1999: Simulations of temperature and turbulence structure of the oceanic boundary layer with the improved near-surface process. *J. Geophys. Res.,* **104,** 15 621–15 634, doi:10.1029/1999JC900068.

Numaguti, A., M. Takahasi, T. Nakajima, and A. Sumi, 1995: Development of an atmospheric general circulation model. *Climate System Dynamics and Modelling,* T. Matsuno, Ed., Vol. 3, University of Tokyo, 1–27.

Polo, I., B. W. W. Dong, and R. T. Sutton, 2013: Changes in tropical Atlantic interannual variability from a substantial weakening of the meridional overturning circulation. *Climate Dyn.,* **41,** 2765–2784, doi:10.1007/s00382-013-1716-x.

Rodríguez-Fonseca, B., I. Polo, J. García-Serrano, T. Losada, E. Mohino, C. R. Mechoso, and F. Kucharski, 2009: Are Atlantic Niños enhancing Pacific ENSO events in recent decades? *Geophys. Res. Lett.,* **36,** L20705, doi:10.1029/2009GL040048.

Smith, T. M., R. W. Reynolds, T. C. Peterson, and J. Lawrimore, 2008: Improvements to NOAA's historical merged land–ocean surface temperature analysis (1880–2006). *J. Climate,* **21,** 2283–2296, doi:10.1175/2007JCLI2100.1.

Suarez, M. J., and P. S. Schopf, 1988: A delayed action oscillator for ENSO. *J. Atmos. Sci.,* **45,** 3283–3287, doi:10.1175/1520-0469(1988)045<3283:ADAOFE>2.0.CO;2.

Sutton, R. T., and D. L. R. Hodson, 2005: Atlantic Ocean forcing of North American and European summer climate. *Science,* **309,** 115–118, doi:10.1126/science.1109496.

Svendsen, L., N. Kvamstø, and N. Keenlyside, 2013: Weakening AMOC connects equatorial Atlantic and Pacific interannual variability. *Climate Dyn.,* doi:10.1007/s00382-013-1904-8, in press.

Timmermann, A., and Coauthors, 2007: The influence of a weakening of the Atlantic meridional overturning circulation on ENSO. *J. Climate,* **20,** 4899–4919, doi:10.1175/JCLI4283.1.

Wang, C. Z., S. F. Dong, and E. Munoz, 2010: Seawater density variations in the North Atlantic and the Atlantic meridional overturning circulation. *Climate Dyn.,* **34,** 953–968, doi:10.1007/s00382-009-0560-5.

Xiang, B. Q., B. Wang, and T. Li, 2013: A new paradigm for the predominance of standing central Pacific warming after the late 1990s. *Climate Dyn.,* **41,** 327–340, doi:10.1007/s00382-012-1427-8.

Yeh, S.-W., and B. P. Kirtman, 2005: Pacific decadal variability and decadal ENSO amplitude modulation. *Geophys. Res. Lett.,* **32,** L05703, doi:10.1029/2004GL021731.

Zhang, R., and T. L. Delworth, 2007: Impact of the Atlantic multidecadal oscillation on North Pacific climate variability. *Geophys. Res. Lett.,* **34,** L23708, doi:10.1029/2007GL031601.